




NUMERICAL MODELLING OF STATIC AEROELASTIC DEFORMATIONS OF SLENDER WING IN AERODYNAMIC DESIGN

Pamela Bugała , Janusz Sznajder  and Adam Sieradzki 

Center of Aviation Technologies, Łukasiewicz Research Network – Institute of Aviation,
Al. Krakowska 110/114, Warsaw 02-256, Poland

Abstract

The article presents the validation of two methods for analyzing the aerodynamic properties of the aircraft wing concerning aeroelastic effects. The first method is based on low-cost computational models (Euler–Bernoulli Beam Model and Vortex Lattice Method [VLM]). Its primary objective is to estimate the wing's deformation early in the design stages and during the automatic optimization process. The second one is a method that uses solutions of unsteady Navier–Stokes equations (URANS). This method suits early design, particularly for unconventional designs or flight conditions exceeding low-fidelity method limits. The coupling of the flow and structural models was done by Radial Basis Functions implemented as a user-defined module in the ANSYS Fluent solver. The structural model has variants for linear and nonlinear wing deformations. Features enhancing applicability for real-life applications, such as the definition of deformable and nondeformable mesh zones with smooth transition between them, have been included in this method. A rectangular wing of a high-altitude long-endurance (HALE) aeroplane, built based on the NACA 0012 profile, was used to validate both methods. The resulting deflections and twists of the wing have been compared with reference data for the linear and nonlinear variants of the model.

Keywords: aeroelasticity; static analysis; beam model; radial basis functions

Type of the work: research article

1. INTRODUCTION

Deformation of a slender wing under steady aerodynamic loads can significantly affect airplane performance. Correctly predicting aerodynamic and aeroelastic effects and implementing design solutions early in developing a new aircraft can bring multiple benefits, such as reduced development costs and time and improved economic efficiency, safety, and comfort. For a slender wing with a high aspect ratio, designers must anticipate and designate several different wing shapes dependent on the angle of attack and load coefficient [1]. These factors are interdependent through the internal structure (stiffness) and loads (aerodynamic and mass). Taking into account static wing deformations is also crucial for determining critical dynamic parameters of the wing, such as flutter speed.

The static aeroelastic analysis is one part of such a large field as wing aeroelasticity, including dynamic phenomena (divergence, flutter) and aerodynamic stability [2]. The aeroelastic analyses mentioned in the article will refer only to static analyses.

Design of a new, competitive aircraft requires balanced use of computational methods for the determination of aerodynamic loads, which may be divided into two categories, the first of them comprising simple, highly reliable, fast-to-apply methods and the second one comprising methods that are more sophisticated, having higher computational cost, and with more precision in terms of sensitivity of results with respect to design parameters, which include aircraft external geometry and internal structure.

The first category of computational methods comprises ‘rapid’ engineering methods, e.g., methods presented in Refs [3,4], taking advantage of collected data obtained in decades of experimental research on aircraft of various layouts and sizes. Also, simple computational methods, such as the Vortex Lattice Method (VLM) or panel methods, based on an assumption of potential flow can be included in this category. These methods can operate on highly simplified aircraft geometry, reduced to airplane planform, mean lines of airfoils, positions and inclination of lifting and control surfaces. Simple computational methods can provide results at low computational costs. However, their accuracy is limited to a narrow range of flight conditions (moderate angle of attack and/or sideslip, excluding transonic Mach numbers).

On the other hand, there is an expressed trend of using higher fidelity methods as early as possible in the project cycle, which can be especially important when designing unconventional structures [5] or considering transonic flow [6]. When optimization of the design concerning performance becomes necessary, sufficient information about aerodynamic characteristics and aircraft loads may be obtained from solutions of RANS equations, which are becoming more and more efficient and friendly in use due to the parallelization of solutions, development of reliable turbulence models (GEKO, Transition-SST), adjoint solvers, and effective meshing techniques, such as polyhedra and overset, which improve the accuracy of gradients of flow variables and speed-up convergence of the solution.

In Ref. [7], several challenges for RANS solvers in aerodynamic design optimization have been mentioned, including ‘robust mesh deformation’. This challenge is addressed in the paper.

Mesh deformation due to geometry displacements during numerical simulations can be accomplished using a body-fitted approach [8], Chimera/overset methods [9], immersed/embedded boundary methods [10], and interpolation methods [11]. Each of them has its own strengths and weaknesses. This work considers a morphing method based on Radial Basis Functions (RBFs) because this methodology has proved robust for large deformations [12].

The primary motivation for considering the topic of static aeroelasticity in this work is to develop and validate two frameworks for aero-structural analysis of flexible wings that can be implemented at the early stage of the project (conceptual design). This goal will be achieved if the computational analysis results (wing performance and deformation) coincide with the benchmark results.

The work focuses on modelling static deformations of high-aspect-ratio wings. The deformations of these wings in the design conditions are large and, therefore, should be considered as early as possible in the design process, including criteria from fields of structural design, performance, stability, and controllability. The high-altitude long-endurance (HALE) aircraft is a special category of airplane with high-aspect-ratio wings and huge wing deflections. The benchmark available in the literature for this type of aircraft was used in the presented work to validate the proposed methods.

A work plan for validating aeroelasticity methods for a wing includes the following steps:

1. Develop two methods (low- and medium-fidelity) for analyzing the aircraft wing’s aerodynamic properties concerning aeroelastic effects.
2. Select validation cases representing flight conditions, wing geometries, and loading scenarios.
3. Perform simulations using the selected aeroelasticity methods on the validation cases.
4. Compare the simulation results to reference solutions.
5. Analyze the results to assess the accuracy and reliability of the aeroelasticity methods.

6. Identify the strengths and limitations of the methods and make recommendations for their use in different types of wing analysis.

The remainder of this paper is structured as follows: Section 2 describes the essential aspects of the tools and methods used in this study. Section 3 describes benchmark geometry and flight conditions. The results are presented and discussed in Section 4 and Section 5 concludes with conclusions and recommendations for future research.

2. DEVELOPED FRAMEWORK/METHODOLOGY

This chapter describes essential aspects of the tools and methods used in this study. The goal of the developed frameworks is to be easy to use and flexible, and the code is designed to be maintainable with provisions for future expansion (optimization tools). It will be validated for the known aeroelastic test case.

The first, low-fidelity framework is X-Foil & AVL wing aeroELasticity (XAVEL) software. XAVEL is an in-house software based on low-cost computing models (Beam Model and VLM). The open-source Athena Vortex Lattice (AVL) and XFOIL programs were used in the aerodynamic module. The beam model was implemented based on the equations presented in the following part of the paper.

The second method is an advanced method that uses a flow model with high complexity and accuracy (ANSYS Fluent) with a structural beam model implemented in user defined function (UDF).

2.1. XAVEL—low-fidelity framework

This chapter presents a simplified method for aeroelastic analysis of the wing, developed using models with low computational cost. The following sections describe the selected models (aerodynamic and structural) and their coupling method. This framework was written in the C programming language and requires the AVL and XFOIL executable program files. In order to use the full computational resources, the developed code has been parallelized, so that all threads of the processor are used during calculations. This allows very fast analysis of multiple computational cases.

2.1.1. Aerodynamic model

The VLM determines wing lifting force and induced drag. The VLM is based on the potential flow theory. By taking into account the Prandtl–Glauert correction, this method has a satisfactory level of accuracy for flight speeds with a Mach number lower than 0.6. The method requires only a coarse definition of the aircraft geometry and the flight state, the simplest general method for 3D aerodynamic analyses of aircraft. Due to few input parameters, analyses can be set up with little effort, and analyses are computationally inexpensive. A detailed formulation of the steady-state and the unsteady variants of VLM can be found in Ref. [13].

The AVL program has been implemented into the aeroelastic platform XAVEL. AVL was created by Mark Drela from MIT Aero & Astro and Harold Youngren [14] and is an open-source program for the aerodynamic and flight-dynamic analysis of rigid aircraft of arbitrary configuration. It employs an extended vortex lattice model for the lifting surfaces, together with a slender-body model for fuselages and nacelles. Extensions of the classic VLM in AVL include accounting for profile drag, calculated in wing sections based on local induced angles of attack and local profile characteristics obtained by other means, experimental or computational.

Another module used in the XAVEL calculations is X-Foil. The X-Foil is an open-source program created by Drela [15] to estimate profile aerodynamic coefficients, including viscous drag. With

the assumption of two-dimensional flow and modelling of boundary layer flow, XFOIL allows for the computation of a total airfoil drag value for the range of angles of attack where flow is attached up to the occurrence of moderate regions of flow separation. This translates into much more accurate predictions of wing performance parameters such as lift-to-drag ratio or energy function.

2.1.2. Structural model

In the proposed approach to the aeroelastic analysis of the wing, the decision was made to use a simplified structural model—a beam model. Beam models used in numerical calculations are usually based on two popular theories—the classical Euler–Bernoulli beam theory and the Timoshenko theory.

An Euler–Bernoulli beam model assumes that sections perpendicular to the beam’s axis remain as such after beam deformation, and it is suitable for medium and high-aspect-ratio beams (aspect ratio higher than 8).

The Euler–Bernoulli beam model is well described in the literature [16–19]. The relationships describing bending and torsional deformations formed the basis for the numerical implementation of the beam model using the C programming language. The finite difference method is used for the beam model’s numerical implementation.

2.1.3. Static analysis

The low-fidelity method uses a two-way interaction between the aerodynamic and structural models. Loading the wing with an aerodynamic force and moment causes the wing to deform, changing the aerodynamic load. Therefore, such a problem must be solved iteratively until the load and deformation match. The implementation of purely one-way coupling often misses the point, as the twisting of the wing directly affects the angle of attack and often changes the wing loading significantly. Figure 1 shows the diagram of two-way fluid-structure interaction implemented in XAVEL.

There are many ways to monitor the convergence of the aforementioned iterative process. In the presented case, the changes of wing angle of attack in successive iterations are observed. A change value below the assumed threshold ends the iterative process. Maintaining a constant lift force coefficient rather than the angle of attack (which is a typical case) has a huge advantage with this type of aeroelastic analysis. It allows to balance the aircraft’s weight and precisely determine envelope points and corresponding deformations.

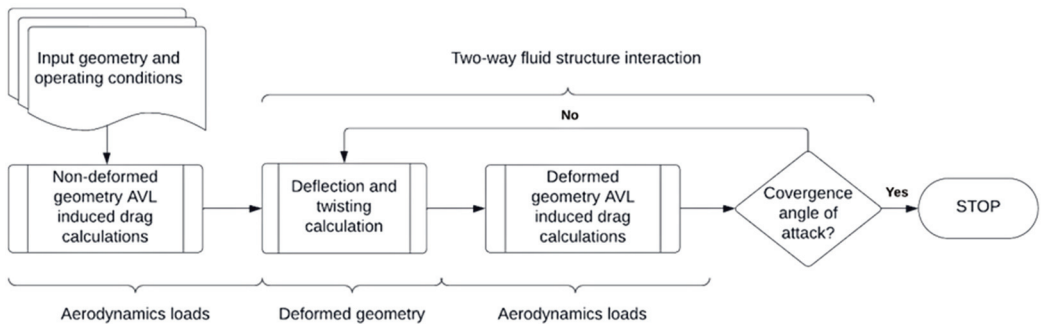


Figure 1. Diagram of two-way fluid-structure interaction implemented in XAVEL. AVL, Athena Vortex Lattice; XAVEL, X-Foil & AVL wing aeroELasticity.

2.2 Medium fidelity framework

This chapter presents a medium-fidelity method for aeroelastic analysis of the wing. The medium-fidelity approach consists of coupling a simplified structural model of a wing (beam model) with a more advanced model of aerodynamics based on numerical solutions of Reynolds-averaged Navier–Stokes equations. For the coupling of the aerodynamic and structural models, the Radial Basis Functions (RBF) [20–22] were implemented as part of the aerodynamic model.

2.2.1. Aerodynamic model

The aerodynamic model described in the previous chapter, based on the VLM method, is restricted to moderate angles of attack and low-to-moderate Mach numbers, which is a serious applicability constraint. For this reason, a more advanced model involving solutions of Reynolds-Averaged Navier–Stokes equations and mesh morphing was prepared to be used with a model for computing deformations of a wing structure. The wider applicability range of numerical solutions of Navier–Stokes equations has a price, being the dependence on a computational mesh for flow volume, which needs to follow the deformations of the solid structure. In the presented work, the main effort on the CFD model concerned the method of modification of the computational mesh in the vicinity of the deformed solid structure. For this purpose, the mesh deformation module using RBF functions was implemented in the ANSYS Fluent software using Dynamic Mesh macros available in the UDF's library. This necessitated the application of the Unsteady Navier–Stokes equations (URANS) solver, although the computational cases used to validate the method consisted of purely steady-flow.

The applied mesh-deformation technique, exploiting Radial Basis Functions, belongs to a category of mesh morphing, which involves morphing of the whole or part of the computational domain following the deformation of its boundary. The most important feature of mesh morphing is that it does not change the number of mesh elements nor the internal structure of the mesh, which means that the structure of the dense layers of elements in the wing boundary layer is preserved after the deformation. In the presented method, morphing is limited to a part of the computational domain, limited by a surface made of points where a mesh deformation coefficient assumes values of zero. The most-often used competing techniques of mesh modification in vicinity of deforming boundary belong to the re-meshing category, which involves destroying parts of the existing mesh and creating new elements. These techniques are used most often in the modelling of store separation and modification of mesh when the domain boundary undergoes discontinuous changes, like the opening of aircraft internal bays. Another technique that could be used in the modelling of deformation of the domain boundary is overset, which involves two meshes in the same domain: the background nondeformable mesh and deforming mesh of smaller size, covering only the vicinity of the deforming boundary. Exchange of information between the two meshes during the solution is conducted in overset interfaces created by the solver. The interfaces are modified if the geometry of the deformable zone changes during the solution. This approach has not been applied in the present work, but is considered for future development of the method.

The RBF re-meshing process involves the following steps:

1. Define source points: Select a set of source points in the domain that will be used to guide the deformation. These points can be located on the surface of the boundary (wing surface) and within the mesh volume, at a distance from the boundary (e.g., to limit the morphing region).
2. Compute displacements: Calculate the displacements of the source points based on the geometry deformation or movement.

3. RBF interpolation: Use the source points and their displacements to interpolate the displacements for the remaining mesh nodes using RBFs. This step involves solving a linear system of equations, where the RBFs act as the interpolating functions.
4. Update mesh nodes: Apply the interpolated displacements to the mesh nodes, resulting in a deformed mesh that conforms to the new geometry of the boundary.

The RBF functions are suitable for interpolation and extrapolation of the deformations. A set of discrete points where deformation is known must be defined. A scalar RBF interpolating/extrapolating function S is defined as:

$$S(x) = \sum_{i=1}^N \eta_i \varphi(\|x - x_i\|) + h(x) \tag{1}$$

where:

N is the number of source points with known deformations, φ is a radial function from a selected basis, being a transformation $\mathbb{R} \rightarrow \mathbb{R}$, $x = [x, y, z]^T$ is a point where S is computed, $x_i = [x_i, y_i, z_i]^T$ is a source point where deformation is known, η_i is an element of a computed vector of coefficients η , and h is a correction polynomial.

The correction polynomial of the order $m-1$, where m , an order of the φ function, is required for the uniqueness of the solution and enables rigid motion of the structure. The interpolating function belonging to basis φ exists if the coefficients η and elements of polynomial h can be found such that the following two conditions are fulfilled:

$$S(x) = G(x_i), 1 \leq i \leq N \tag{2}$$

where $G(x_i)$ is a known value at point x_i . In the presented method, $G(x_i)$ is a component of boundary deformation, namely translation of point x_i along each one of the coordinate axes.

The second condition is an orthogonality condition for all polynomials p with a degree less or equal to the degree of the polynomial h :

$$\sum_{i=1}^N \eta_i p(x_i) = 0 \tag{3}$$

If the order of function φ is $m \leq 2$, then in the three-dimensional space, a polynomial h may be applied, of the form:

$$h(x) = \beta_1 + \beta_2 x + \beta_3 y + \beta_4 z \tag{4}$$

The values of coefficients η and β may be determined from the solution of the system of order N :

$$\begin{pmatrix} U & P \\ P^T & 0 \end{pmatrix} \begin{pmatrix} \eta \\ \beta \end{pmatrix} = \begin{pmatrix} G \\ 0 \end{pmatrix} \tag{5}$$

where:

$G = \{G_1, \dots, G_N\}^T$ are known values of interpolation function in source points, and $\beta = \{\beta_1, \dots, \beta_N\}^T$ are coefficients of polynomial h .

U is interpolation matrix $N \times N$, dependent on the distances between points:

$$U_{ij} = \varphi\left(\|x_i - x_j\|\right), 1 \leq i \leq N, 1 \leq j \leq N;$$

\mathbf{P} is a constraint matrix of the form:

$$\mathbf{P} = \begin{pmatrix} 1 & x_1 & y_1 & z_1 \\ 1 & x_2 & y_2 & z_2 \\ \vdots & \vdots & \vdots & \vdots \\ 1 & x_N & y_N & z_N \end{pmatrix}. \quad (6)$$

In the described implementation of RBF functions, the interpolated variables (scalars S in Eq. (1)) are components of transitions of the nodes of the computational mesh:

$$\begin{aligned} d_x &= S_x(x) = \sum_{i=1}^N \eta_{xi} \varphi(\|x - x_i\|) + \beta_{x1} + \beta_{x2}x + \beta_{x3}y + \beta_{x4}z, \\ d_y &= S_y(x) = \sum_{i=1}^N \eta_{yi} \varphi(\|x - x_i\|) + \beta_{y1} + \beta_{y2}x + \beta_{y3}y + \beta_{y4}z, \\ d_z &= S_z(x) = \sum_{i=1}^N \eta_{zi} \varphi(\|x - x_i\|) + \beta_{z1} + \beta_{z2}x + \beta_{z3}y + \beta_{z4}z. \end{aligned} \quad (7)$$

The node translations described above depend on translations defined in source points, which need not be mesh nodes. It makes the method mesh-independent, which feature in Refs [20, 21], and is called ‘meshless’. The other important feature of the method is the possibility of application in parallel computations on computer nodes when each computational thread has access to only a part of the computational mesh. It requires only sending to each computational process tables of source points, and coefficients η and β which can be determined in the host process of the computations.

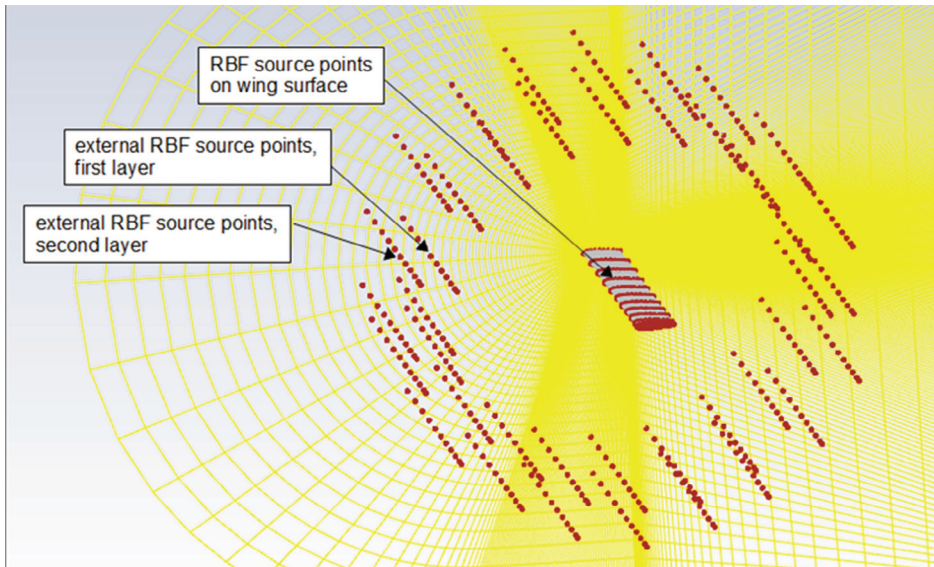


Figure 2. An example distribution of RBF source points on the wing surface and at a distance from it, where mesh deformation vanishes. RBF, radial basis functions.

Two groups of source points are defined in the described implementation of RBF functions. The first group consists of points on the wing surface and the other group consists of points at some distance from the surface, where it is desired to end the deformable region of the mesh and keep the remaining region intact. This is shown in Fig. 2, where the dense distribution of source points on the wing surface in the center is surrounded by two layers of source points at some radial distance, in order to end the deformable zone.

The source points, which are located on the wing surface, are distributed in chordwise rows, with density increasing at leading and trailing edges, as shown in Fig. 3. In the conducted analyses, 20–50 points in a row were used, and the number of rows was 10–20.

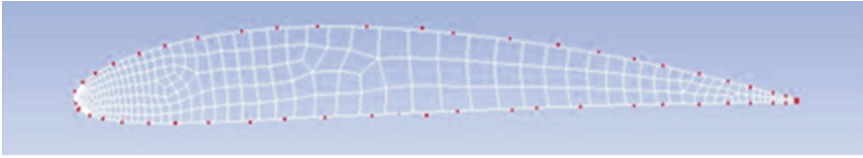


Figure 3. Distribution of RBF points along the wing chord (view from the side edge of the wing). RBE, radial basis functions.

The mesh deformations produced by wing deformation must vanish in the space between the layers of the source points external to the wing, visible in Fig. 3. This is accomplished by introducing an additional mesh deformation coefficient d . The function defining its distribution is given in the cylindrical coordinate system with a longitudinal axis along span and spherical at the wing tip:

$$\begin{aligned}
 d &= 1 \text{ if } \vec{r} \in (0, \vec{r}_0), \\
 d &= 0.5 \cdot \left(1 + \cos \left(\frac{\vec{r} - \vec{r}_0}{\vec{r}_1 - \vec{r}_0} \cdot \pi \right) \right) \text{ if } \vec{x} \in (\vec{r}_0, \vec{r}_1), \\
 d &= 0 \text{ if } \vec{r} > \vec{r}_1,
 \end{aligned} \tag{8}$$

where r_0 and r_1 are the radii of the two layers of external source points.

The final mesh deformation in a point in the flow domain is the product of the deformation computed with Eq. (7) and the mesh deformation coefficient defined by Eq. (8). This assures the mesh deformation is continuous and decreases to zero in the desired region. The volume where the value of d is higher than zero is thus a part of the computational domain subject to morphing.

The spatial distribution of coefficient d computed for an exemplary rectangular wing of aspect-ratio 5 is shown in Fig. 4. For demonstration purposes, the wing has been subject to a deformation resulting in wing-tip translation in the normal direction of 5% span. The spatial distribution of node translation in the direction normal to the wing planform of the same wing is shown in Fig. 5 as isolines of constant translation. The translations are presented in two perpendicular planes: one plane along the wing span and another along the wing chord, in approximately 0.7 half-span. In Fig. 6 is presented the cross-section of the domain in a plane located in the wing half-chord, and presenting details of the mesh. The resulting distribution of node translations shows that the goal of ensuring continuous, smooth distribution of node deformation, vanishing at a prescribed distance from the deforming structure, has been reached.

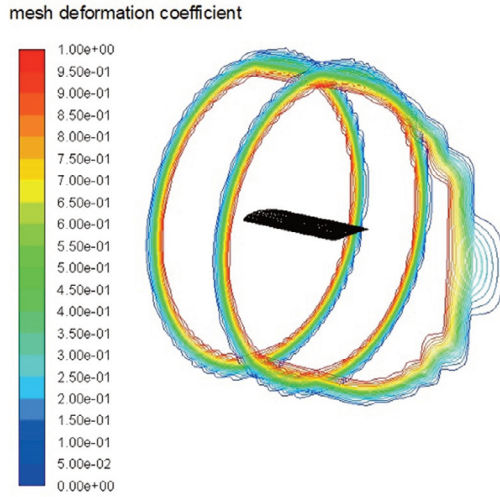


Figure 4. Contour of the spatial distribution of mesh deformation coefficient, computed for mesh nodes between radii r_0 and r_1 of Eq. (8).

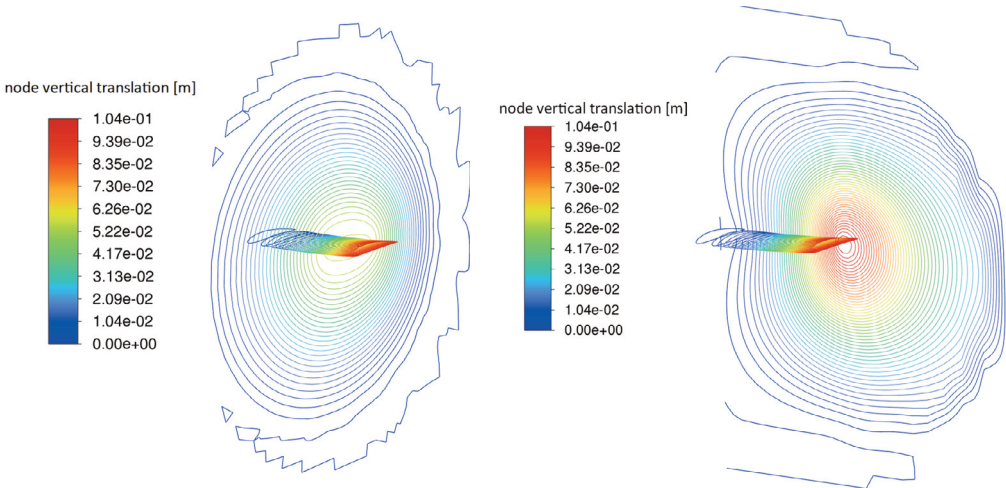


Figure 5. Distribution of mesh node translations (in meters) in two planes perpendicular to wing chordplane.

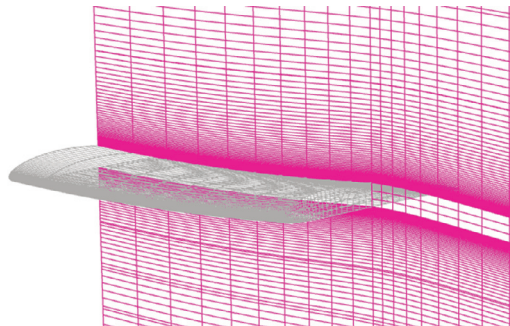


Figure 6. Mesh deformation in the middle-chord plane, following wing deformation.

The mesh deformation is initiated by the import to the solver of the set of source points located on the deformed surface. Then the system of Eq. (5) is solved in the host process of ANSYS Fluent in order to determine the vectors of coefficients η and β . These vectors are then sent to the parallel processes operating on fragments of the domain. The deformation, described by Eqs. (7) and (8), is conducted by the solver executing a user-defined function using the macro DEFINE_GRID_MOTION of ANSYS Fluent solver during the prescribed number of time steps.

2.2.2. Structural model

A finite-element beam model, described in Ref. [23], was used to discretize the structure of the wing and to determine the deformations under aerodynamic loads. The beam model includes the following parameters at the nodes of the elements:

- longitudinal displacements u_1, u_2 ,
- transverse displacements v_1, v_2, w_1, w_2 ,
- torsion angles $\varphi_{x,1}, \varphi_{x,2}$,
- deflection angles (rotation of sections about the transverse axes) $\varphi_{y,1}, \varphi_{y,2}, \varphi_{z,1}, \varphi_{z,2}$

The stiffness matrix of an element has size 12 by 12, and its elements are dependent on tensile stiffness, EA, bending stiffness in two planes: EJ_y, EJ_z , and torsional stiffness, GK, which may be determined analytically, e.g., by methods described in [23]. The stiffness matrix of the beam element has the form [21]:

$$\begin{bmatrix}
 \frac{EA}{l} & & & & & & & & & & & \\
 0 & \frac{12EJ_z}{l^3} & & & & & & & & & & \\
 0 & 0 & \frac{12EJ_y}{l^3} & & & & & & & & & \\
 0 & 0 & 0 & \frac{GK_s}{l} & & & & & & & & \\
 0 & 0 & 0 & 0 & \frac{4EJ_y}{l} & & & & & & & \\
 0 & 0 & 0 & 0 & 0 & \frac{4EJ_z}{l} & & & & & & \\
 \frac{-EA}{l} & 0 & 0 & 0 & 0 & 0 & \frac{EA}{l} & & & & \text{Symmetry} & \\
 0 & \frac{-12EJ_z}{l^3} & 0 & 0 & 0 & \frac{-6EJ_z}{l^2} & 0 & \frac{12EJ_z}{l^3} & & & & \\
 0 & 0 & \frac{-12EJ_y}{l^3} & 0 & 0 & 0 & 0 & 0 & \frac{12EJ_y}{l^3} & & & \\
 0 & 0 & 0 & \frac{-GK_s}{l} & 0 & 0 & 0 & 0 & 0 & \frac{GK_s}{l} & & \\
 0 & 0 & \frac{-6EJ_y}{l^2} & 0 & \frac{2EJ_y}{l} & 0 & 0 & 0 & 0 & 0 & \frac{4EJ_y}{l} & \\
 0 & \frac{6EJ_z}{l^2} & 0 & 0 & 0 & \frac{2EJ_z}{l} & 0 & \frac{-6EJ_z}{l^2} & 0 & 0 & 0 & \frac{4EJ_z}{l}
 \end{bmatrix} \tag{9}$$

The rows and columns of the stiffness matrix correspond to the node parameters described above. They may be interpreted as forces and moments created by unit displacements or rotations in the respective nodes.

The stiffness matrix of the beam is composed of matrices for single elements by adding contributions of each element's stiffness in the rows of the global matrix, corresponding to degrees of freedom in the nodes of the discretized wing. In order to take into account the geometric orientation of elements (a wing may be segmented, with varying dihedral, sweep, twist), each element matrix is first transformed to a beam coordinate system by multiplication by transformation matrices composed of directional cosines of element axis [24].

The finite element method also requires that continuous loads on wing surfaces are reduced to discrete loads in the beam nodes, corresponding to the node degrees of freedom. This is done based on the principle of equality of work of external and internal forces on virtual displacements [24].

Application of boundary conditions in the present case assumes zero nodal linear and angular deflection in particular nodes and directions, e.g., zero deflection and rotation at the wing root. It means that the corresponding rows and columns of the global stiffness matrix are removed from the system.

The wing deformation, consisting of translations and rotations in the element nodes, are determined by the solution of the system:

$$\{X\} = [K]^{-1} \cdot \{F\}, \quad (10)$$

where $\{X\}$, deformation vector; $[K]^{-1}$, inverse stiffness matrix; and $\{F\}$, nodal force vector.

Depending on the problem, the analysis may be conducted in a one-step fashion, by the one-time solution of the system (1), or, in order to account for the nonlinear behavior of the structure, by performing the solution in more steps. The first option is suitable for relatively stiff wings and moderate deformations. In many cases, e.g., high aspect-ratio wings undergoing large deflections, it is necessary to account for nonlinear effects in the deformations. This is conducted in the presented method by application of the predictor–corrector procedure. The stiffness matrix is computed for the nondeformed beam in the predictor step. The system (10) is solved, the deformations are halved, and applied in the nodes, in order to compute the stiffness matrix of the deformed structure for the corrector step. Then the system (10) is solved again, and the deformations are applied to the original, nondeflected beam. As a final step in the structural analysis, the nodal parameters computed for the nodes on the wing (beam) axis are used to compute the displacements in the RBF source points located on the wing surface. This process includes translations of the RBF points along beam axes and rotations of the wing cross-sections as a result of wing bending and twist. This is shown in Fig. 7.

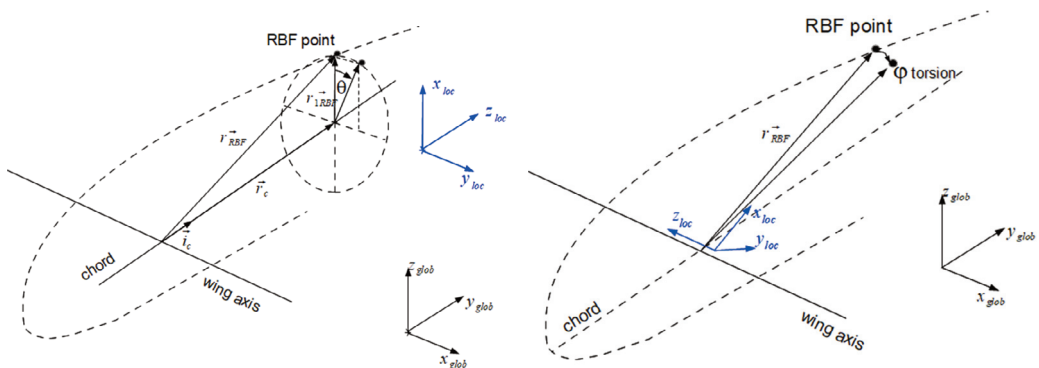


Figure 7. Deformations of wing cross-sections hosting RBF source points as a result of bending of wing axis (left fragment) and twist (right fragment). RBF, radial basis functions.

3. BENCHMARK

The following section describes a reference case, a wing of a HALE aircraft. The selected benchmark case was also analyzed in Ref. [25] and contains all the necessary information to conduct analyses with the developed methods.

It is a simple rectangular wing with profile NACA 0012. The calculations presented in Ref. [25] were carried out by combining the panel method and the nonlinear load determination method. Table 1 shows the geometry and structural properties of the wing of the validation case. Gravitational forces were not included in the calculations.

Table 1. Geometry and structural properties of the validation case wing [25].

Wing properties	Study value
Semi-span [m]	16
Chord [m]	1
Center of gravity	Mid-chord
Elastic axis	Mid-chord
Inertia about mid stiffness [Nm ²]	0.1
Torsional stiffness [Nm ²]	1×10^4
Bending stiffness [Nm ²]	2×10^4
Edgewise stiffness [Nm ²]	5×10^6

The calculations were carried out for a flight at an altitude of 20,000 m at a speed of 25 m/s at a 2° and 4° angle of attack. The wing deflection, twist, and lift distribution will be compared to verify the two methods with the reference case.

4. RESULTS

The first case considered was a cruise-compatible flight condition and the second case considered was a flight condition resulting in a larger aeroelastic response.

Figures 8 and 9 show bending and twisting along the span calculated in XAVEL and published in Ref. [25]. The deflection and torsion of the wing obtained from the simplified method calculations agree with the results presented in both validation cases. The results for angle $\alpha = 2^\circ$ coincide with the validation case perfectly.

In the case of the angle of attack $\alpha = 4^\circ$, the wing deflection coincides with the validation results, while in the case of the twist, the difference does not exceed 10%. The reason for the lower twist for the linear model in XAVEL than for the nonlinear model in the benchmark is unknown. In XAVEL, the effect of ‘shortening’ the wing is a matter of proper postprocessing of data from the analysis—recalculating nodes’ positions assuming a constant span of individual sections (elements) of the wing. In contrast, the benchmark of the wing is modelled as a geometrically exact beam. Patil and Hodges [26] showed that the nonlinear structures played an important role in flight conditions resulting in a large aeroelastic response.

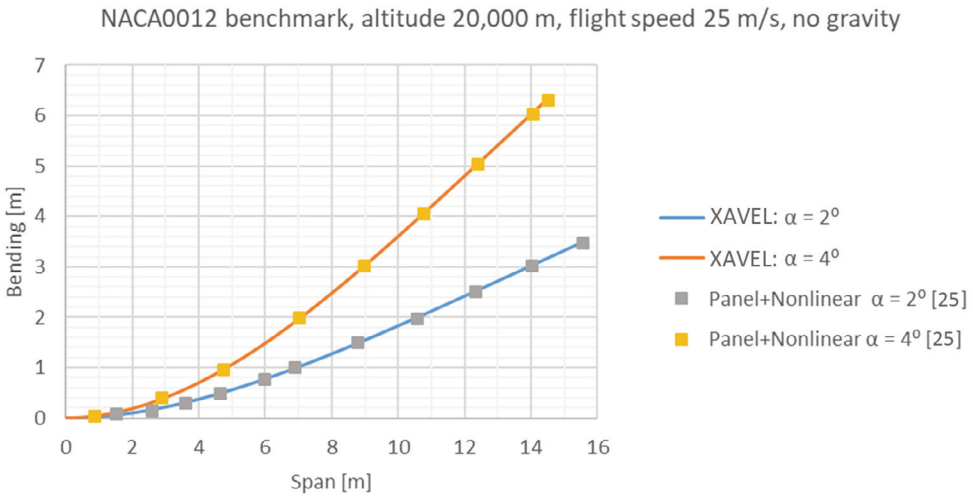


Figure 8. Static aeroelastic solution for a flight condition of 20,000 m altitude, 25 m/s, and an $\alpha = 2^\circ$ and $\alpha = 4^\circ$. XAVEL, X-Foil & AVL wing aeroELasticity.

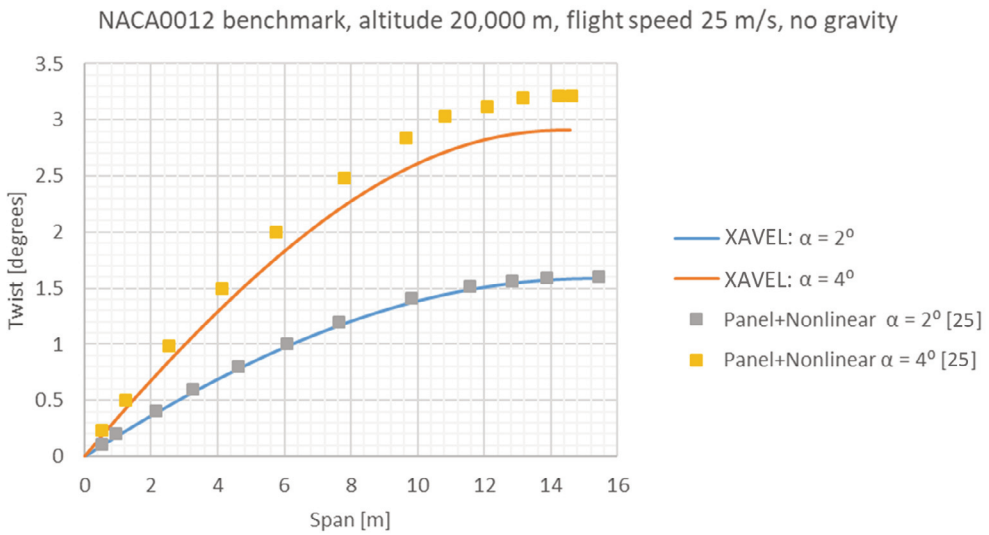


Figure 9. Static aeroelastic solution for a flight condition of 20,000 m altitude, 25 m/s, and an $\alpha = 2^\circ$ and $\alpha = 4^\circ$. XAVEL, X-Foil & AVL wing aeroELasticity.

Figure 10 shows lift distributed along the span calculated in XAVEL and published in Ref. [25]. The force distribution obtained with the XAVEL program is consistent with the results obtained in Ref. [25].

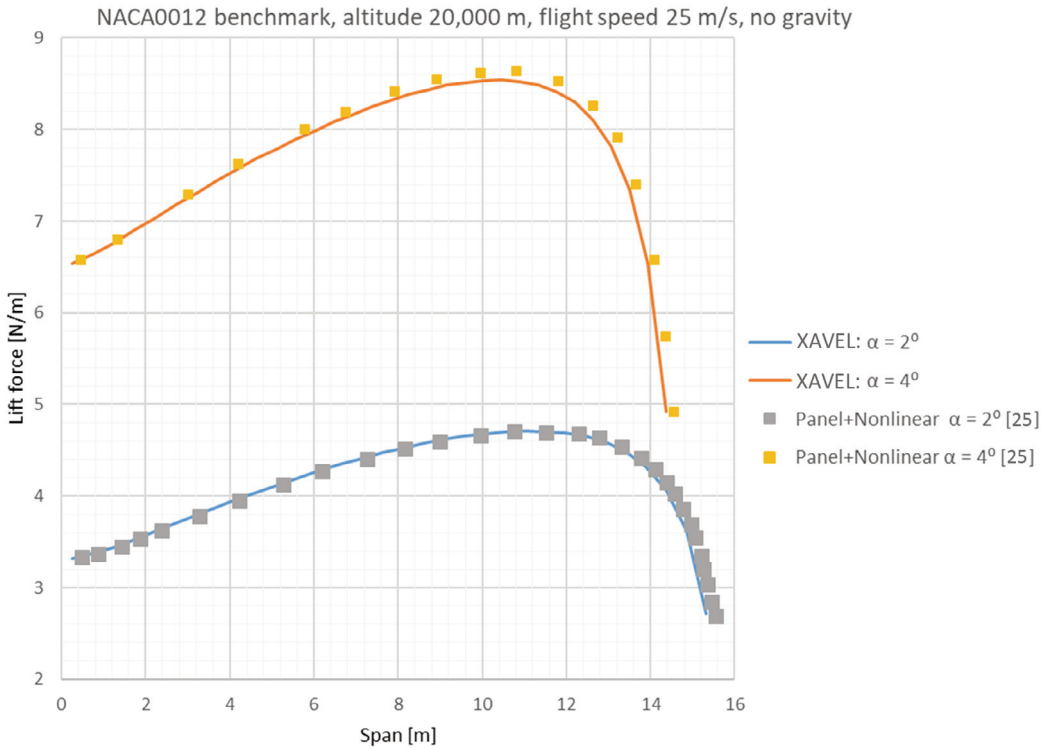


Figure 10. Lift force for a flight condition of 20,000 m altitude, 25 m/s, and an $\alpha = 2^\circ$ and $\alpha = 4^\circ$. XAVEL, X-Foil & AVL wing aeroElasticity.

It can therefore be concluded that the simplified method is pretested and validated.

The medium-fidelity aero-structural model involving solutions of URANS flow equations and RBF functions for the interpolation of mesh deformation has been validated on the same rectangular wing of aspect-ratio 32 and NACA 0012 airfoil. The flow conditions were altitude 20,000 m, $\alpha = 2^\circ$ and 4° , $V = 25$ m/s. Both linear and nonlinear models of beam deflections were applied. The obtained results have been compared with the results provided in Ref. [25], including two different flow models: potential flow, solved by panel methods, and the second model: Euler flow equations. Accordingly, with the approach taken in Ref. [25], the mass of the wing was omitted, resulting in artificially augmented wing deflection to make differences between the results of different methods more visible. A structural mesh consisting of 0.8 mln of hexahedral elements has been applied in the current URANS + RBF + FEM approach, enabling relatively easy control of the number of elements and their quality.

The wing deformation was determined in an iterative fashion in the linear and nonlinear approaches. In either approach, the first step of the coupled aero-structural analysis started with the determination of the aerodynamic loads of the undeformed wing. Then the wing deformation was determined, which in the linear approach involved a single solution of the Eq. (8). In the nonlinear approach, Eq. (8) was solved twice; first in the predictor step, having stiffness matrix computed for undeformed structure, and then in the corrector step, having stiffness matrix computed for the half-deformed wing. Then in either approach, the translation of RBF source points was computed based on beam node translations. This ended the computational step of the coupled analysis. Each next computational step of aero-structural analysis started from reading into the Fluent solver of original, undeformed geometry and applying

translations in the RBF source points computed in the previous step. This triggered the deformation of the mesh involving wing surface nodes and mesh nodes in the deformable region. The mesh deformation process was conducted in parallel with the flow solution during many initial time steps of the flow solution, and the flow solution converged for the deformed wing structure. Then, the new beam deflection was conducted in a linear or nonlinear fashion by application of the new approximation of aerodynamic loads to the original beam. The process converged within a few steps, as shown in Fig. 11. The iterations were stopped when relative change of displacement and twist in the last wing cross-section decreased below 2% of the current-step values.

The wing deflection in the deformed mesh, computed with the present method, is shown in Fig. 12. The comparison of the obtained results with the results provided in Ref. [25] is shown in Fig. 13 for wing bending and in Fig. 14 for wing twist.

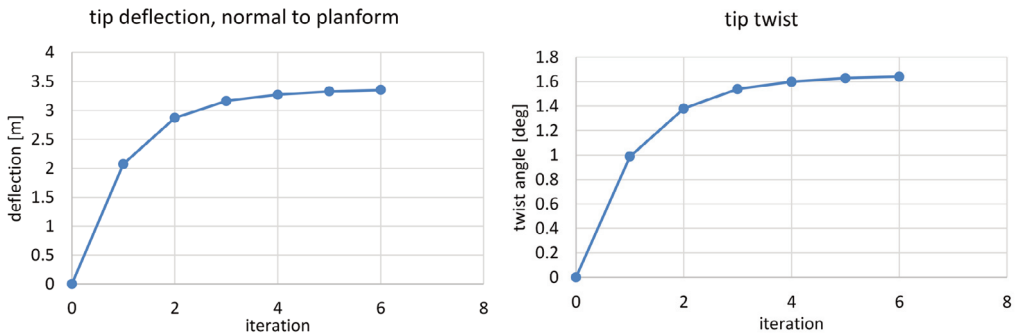


Figure 11. Convergence of the iteration process of aero-structural analysis.

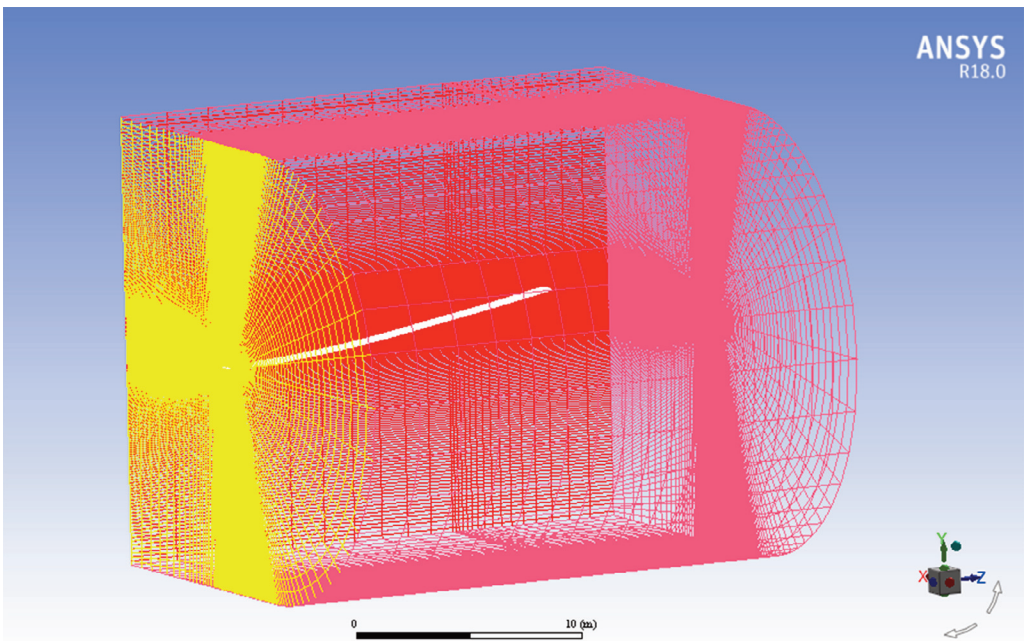


Figure 12. Deflection of the test wing computed with the URANS + RBF + FEM approach. RBF, radial basis functions; URANS, unsteady Navier-Stokes equations.

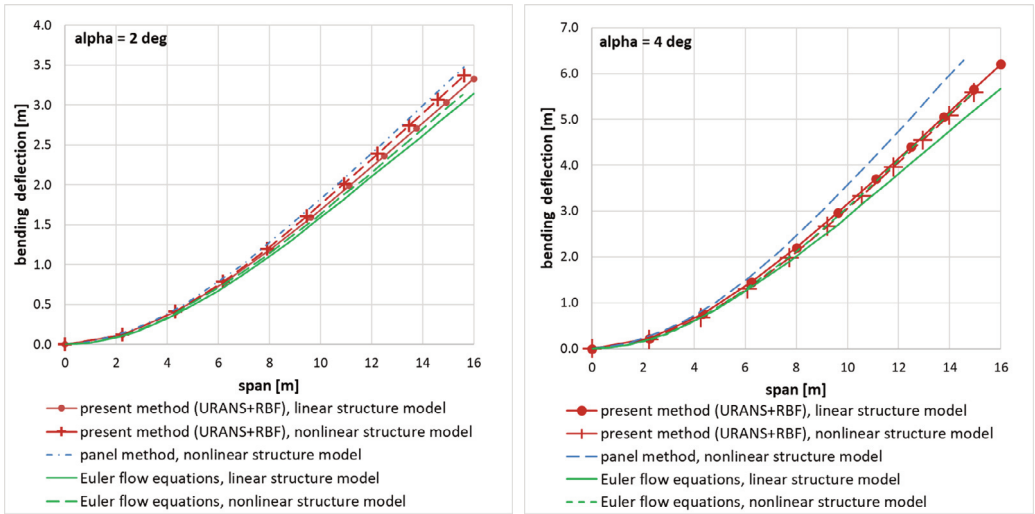


Figure 13. Comparison of bending deflection of the test wing, normal to wing planform, computed using the present method with results of Ref. [25]. RBF, radial basis functions; URANS, unsteady Navier-Stokes equations.

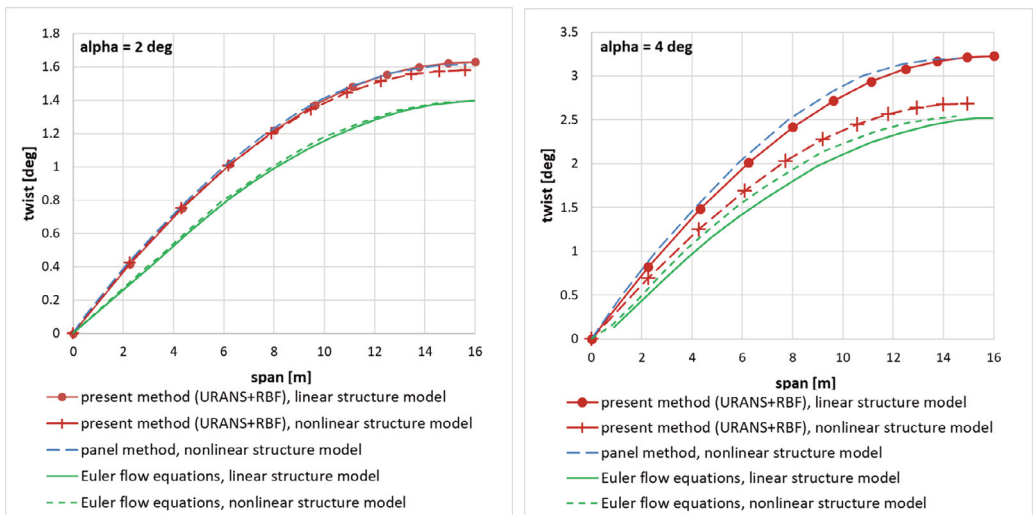


Figure 14. Comparison of twist of the test wing, computed using the present method with results of Ref. [25]. RBE, radial basis functions; URANS, unsteady Navier-Stokes equations.

In comparing the results of the present method with the results of work [25], a good agreement can be found between the results of the present approach and the reference data. The results—wingtip deflection and twist—obtained with the present structural model and aerodynamic loads computed solving URANS equations are within the limits of the solutions obtained by authors of work [25], where two different (inviscid) flow models were applied. For these low values of angle of attack, flow viscosity has minor impact on lift, so such a proximity of results should be expected. In both sets of results, the nonlinear structural model predicts an inward deflection of the wing tip, as opposed to linear solutions, where the wing tip stays in the same plane during deformation.

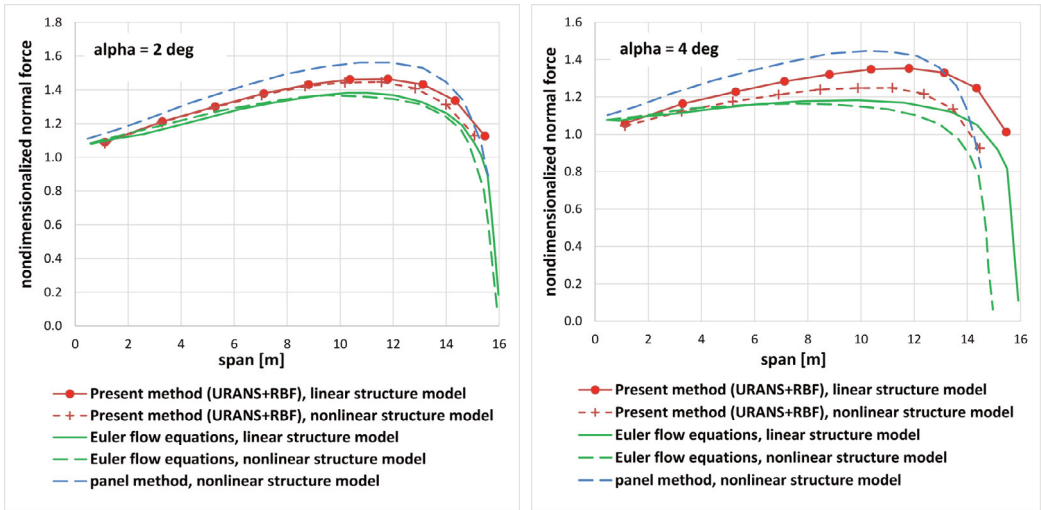


Figure 15. Comparison of distributions of non-dimensionalized normal force computed using the present method with results of [25]. RBF, radial basis functions; URANS, unsteady Navier-Stokes equations.

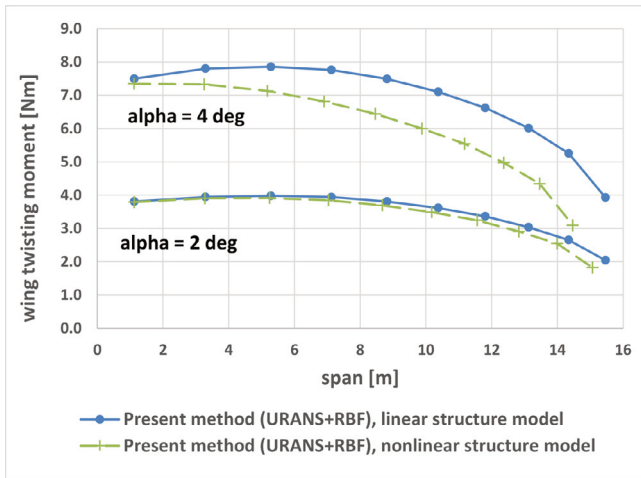


Figure 16. Comparison of distributions of wing twisting moment computed with the present method using the linear and nonlinear variant of the structure model. RBF, radial basis functions; URANS, unsteady Navier-Stokes equations.

It can be seen that the wing deformations obtained with the present method (URANS + RBF) are consistent with the results of wing loading computed in wing strips. In Fig. 15 is shown a comparison of the distribution of non-dimensionalized normal force computed with the present method and methods of Ref. [25], scanned from this reference. The force non-dimensionalization was conducted as in Ref. [25] using a two-dimensional flat plate curve slope and wing angle of attack. By comparing the results of Figs. 13 and 15, each beam deflection is in similar relations to other deflections, as are the distributions of the normal force. A noticeable feature of the solution obtained with the present method (URANS + RBF) at $\alpha = 4^\circ$ is the lower wing twist computed by the present nonlinear structure model with respect to the result of the linear one, which is not the case in the results of Ref. [25]. In the present approach, the distribution of twisting moment over the wing in the nonlinear solution, shown in Fig. 15,

has lower values than the distribution of twisting moment in the linear solution, which is in accordance with the respective distributions of the normal force. It should be noted, however, that the results of wing twist obtained for this angle of attack are within the limits of the results of various approaches presented in Ref. [25]. The likely cause of the mentioned differences in wing deformations, especially the wing twist, are differences in the applied structural models of the wing. This phenomenon will be investigated further in the development of the present method.

5. CONCLUDING REMARKS AND FUTURE WORK

The two presented methods of aeroelastic analysis of airplane wings are intended for application in the early and medium stages of aircraft design when details of its geometry are not fixed and the number of considered variants is large. In the structural model, both methods use spanwise distributions of bending and torsional stiffness rather than discretization of internal structure. Both methods have produced results that agree closely with benchmark results for very flexible wings with artificially increased deflection (by omitting gravity). The two methods complement each other in terms of their field of applicability. The first one, due to its aerodynamic model based on panel methods, is mainly suitable for designing low-speed, medium-high aspect-ratio wings. The simple aerodynamic model allows for application in design and optimization with explicitly defined design points in terms of lift and flight velocity. The simple computational model produces results quickly, making it suitable for automated optimization or analysis in batch processing. The second method, owing to the flow solution obtained by the RANS equations, overcomes many potential limitations of the flow models applied in AVL and XFOIL software. It can be used for a wider range of flow velocities, angles of attack, and sideslip. The additional complexity of the method involves more manual input, e.g., during initial mesh generation for new geometry. However, this process is also largely automated due to the capabilities of Ansys Meshing software. In the present implementation, the grid modification algorithm is linked to the beam model calculating displacements of wing surface points. However, it can be linked to other models of computing structural displacements.

Future work will include applying the developed methods in optimizing wing structure for performance under design loads, implementing a nonlinear model for structure analysis in the XAVEL software, and validating the developed methods based on more experimental studies. There is a general need for more reliable data in the literature to benchmark static aeroelastic analysis programs. Most of the literature reviews modal flutter calculations without information on wing stiffnesses or mass distribution. By validating the method, it will be possible to implement it in an optimization environment.

REFERENCES

- [1] Zuo, Y., Chen, P., Fu, L., Gao, Z., and Chen, G. "Advanced Aerostructural Optimization Techniques for Aircraft Design", *Mathematical Problems in Engineering* (2015): pp. 1–12. DOI 10.1155/2015/753042.
- [2] Bisplinghoff, L. Raymond, Holt, Ashley, and Halfman, L. Robert, *Aeroelasticity*, Courier Corporation (2013).
- [3] Lan, Chuan-Tau Edward Lan and Roskam, Jan. *Airplane Aerodynamics and Performance*, Roskam Aviation and Engineering (1997).
- [4] Raymer, Daniel. *Aircraft Design: A Conceptual Approach*, Fifth Edition, American Institute of Aeronautics and Astronautics, Inc., Washington, DC. (2012). DOI 10.2514/4.869112.
- [5] Karpuk, Stanislav, Liu, Yaolong, and Elham, Ali. "Multi-fidelity Design Optimization of a Long-range Blended Wing Body Aircraft with New Airframe Technologies", Vol. 7 No. 7 (2020): p. 87. DOI 10.3390/aerospace7070087.
- [6] Bons, P. Nicolas, and Martins, R. R. A. Joaquim. "Aerostructural Design Exploration of a Wing in Transonic Flow", Vol. 7 No. 8 (2020): p. 118. DOI 10.3390/aerospace7080118.

- [7] Martins, R. R. A. Joaquim, 2022, “Aerodynamic Design Optimization: Challenges and Perspectives”, *Computers & Fluids* Vol. 239 (2022): p. 105391. DOI 10.1016/j.compfluid.2022.105391.
- [8] Zhang, Yaoxin, and Jia, Yafei. “2D Automatic Body-fitted Structured Mesh Generation Using Advancing Extraction Method”, *Journal of Computational Physics* Vol. 353 (2018): pp. 316–335, DOI 10.1016/j.jcp.2017.10.018.
- [9] Reinbold, Christopher, Sørensen, Kaare, and Breitsamter, Christian. “Aeroelastic Simulations of a Delta Wing with a Chimera Approach for Deflected Control Surfaces”, *CEAS Aeronautical Journal* Vol. 13 No. 1 (2022): pp. 237–250. DOI 10.1007/s13272-021-00561-3.
- [10] Feuillet, Rémi, Adrien Loseille, and Frédéric Alauzet. “Mesh Adaptation for the Embedded Boundary Method in CFD”, Research Report n°9305, Research Centresaclay – Île-De-France, Palaiseau, Nov. 2019. DOI 10.13140/RG.2.2.22343.44969.
- [11] Selim, M., and Koomullil, R. P., 2016, “Mesh Deformation Approaches – A Survey”, *Journal of Physical Mathematics* Vol. 7 No. 2 (2016): 1000181. DOI 10.4172/2090-0902.1000181.
- [12] Biancolini, E. Marco, Viola, M. Ignazio and Riotte, Matthieu. “Sails Trim Optimisation Using CFD and RBF Mesh Morphing”, *Computer & Fluids*, Vol. 93 No. 2 (2014): pp. 46–60. DOI 10.1016/j.compfluid.2014.01.007.
- [13] Katz, Joseph and Plotkin, Allen. *Low-speed Aerodynamics*, Cambridge University Press, Cambridge (2001). DOI 10.1017/cbo9780511810329.
- [14] Drela, Mark and Youngren, Harold “AVL Overview.” [Online]. Available: <https://web.mit.edu/drela/Public/web/avl/> [Accessed: 16-Jun-2020]
- [15] Drela, Mark, “XFOIL.” [Online]. Available: <https://web.mit.edu/drela/Public/web/xfoil/> [Accessed: 13-Sep-2020].
- [16] Andersen, Lars, and Nielsen, R. K. Søren. “Elastic Beams in Three Dimensions”, *DCE Lecture Notes*, Vol. 1 No. 23 (2008): p. 104. [Online]. Available: <http://homes.civil.aau.dk/jc/FemteSemester/Beams3D.pdf>
- [17] Megson, T. H. G. *Aircraft Structures for Engineering Students*, Fifth Edition. Amsterdam: Elsevier (2012). DOI 10.1016/C2009-0-61214-9.
- [18] Young, C. Warren, Budynas, G. Richard, and Sadegh, M. Ali. *Roark’s Formulas for Stress and Strain*, McGraw-Hill Companies, New York (2012).
- [19] Bauchau, O. A., and Craig, J. I. “Structural Analysis: With Applications to Aerospace Structures”, Part of: *Solid Mechanics and its Applications* Vol. 163. Springer, New York (2009).
- [20] Biancolini, Marco Evangelos. *Fast Radial Basis Functions for Engineering Applications*, Springer International Publishing, Rome (2017). DOI 10.1007/978-3-319-75011-8.
- [21] Schaback, A. Robert, Chen, C. S., and Hon, Y. C. *Scientific Computing with Radial Basis Functions*, University of Southern Mississippi, Hattiesburg (2005).
- [22] Cella, Ubaldo. “Setup and Validation of High Fidelity Aeroelastic Analysis Methods Based on RBF Mesh Morphing”. PhD Thesis, University of Rome “Tor Vergata,” Rome. 2017. [Online]. Available: <http://ribes-project.eu/Documents/PhDthesis-UbaldoCella.pdf> [Accessed: 05-Jun-2022].
- [23] Brzoska, Zbigniew. *Statyka i stateczność konstrukcji prętowych i cienkościennych* (English title: *Statics and Stability of Rod-like and Thin-walled structures*). Państwowe Wydawnictwo Naukowe (1965).
- [24] Rakowski, Gustaw and Kacprzyk, Zbigniew. *Metoda elementów skończonych w mechanice konstrukcji* (English title: *Finite Element Method in Mechanics of Structures*). Oficyna Wydawnicza Politechniki Warszawskiej (2016).
- [25] Smith, J. Marylin, Patil, J. Mayuresh and and Hodges, H. Dewey. “Cfd-based Analysis of Nonlinear Aeroelastic Behavior of High-aspect Ratio Wings”, *19th AIAA Applied Aerodynamics Conference, American Institute of Aeronautics and Astronautics Inc.*, 11–14 June 2001, pp. 1–10. DOI 10.2514/6.2001-1582.
- [26] Patil, J. Mayuresh and Hodges, H. Dewey. “On the Importance of Aerodynamic and Structural Geometrical Nonlinearities in Aeroelastic Behavior of High-aspect-ratio Wings”, *41st Structures, Structural Dynamics, and Materials Conference and Exhibit*, 03–06 April 2000, pp. 905–915. DOI 10.2514/6.2000-1448.